

Transferability of force fields for 2D silicon (silicene)

Marcin Maździarz*

Address: Department of Computational Science, Institute of Fundamental Technological Research Polish Academy of Sciences, Pawińskiego 5B, 02-106 Warsaw, Poland

Email: Marcin Maździarz - mmazdz@ippt.pan.pl

* Corresponding author

Abstract

An ability of various interatomic potentials to reproduce the properties of silicene (2D silicon) polymorphs were examined. Structural and mechanical properties of the flat (FS), low-buckled (LBS), trigonal dumbbell (TDS), honeycomb dumbbell (HDS) and large honeycomb dumbbell (LHDS) single-layer silicon (silicene) phases, were obtained using density functional theory (DFT) and molecular statics (MS) calculations with Tersoff, MEAM, Stillinger-Weber, EDIP, ReaxFF, COMB and machine-learning-based (ML-IAP) interatomic potentials. A quantitative systematic comparison and discussion of the results obtained are reported.

Keywords

2D materials; Silicene; Interatomic potentials; Force fields; DFT; Mechanical properties

1 Introduction

We live in the "Silicon Age" due to the great importance of elemental silicon to the modern global economy, it is mainly about electronics. Silicon is one of the best investigated materials and the quality of its production is impressive. However, this applies to bulk silicon. The interest in the graphene has also led to interest in other non-carbon 2D materials [1,2]. One such material is precisely the 2D silicon called silicene [3,4]. Using first-principles methods, with current com-

puter resources, we can model structures up to about a few hundred atoms. For larger systems, we need approximate methods, e.g. molecular dynamics/statics. For these methods, the quality of the interatomic potentials (IAPs) used is crucial. Because of the importance of silicon, but also its complexity, dozens of potentials have been proposed for it. In the very well-known NIST Interatomic Potentials Repository, there are 27 potentials for silicon (no other element has more potentials), the oldest one from 1985 and the latest from 2020 [5]. At least five 2D silicon polymorphs have been reported in the literature, that is, flat (FS), low-buckled (LBS) [6], trigonal dumbbell (TDS), honeycomb dumbbell (HDS) and large honeycomb dumbbell (LHDS) [7]. There are still doubts about their dynamic stability, e.g. for a flat phase the negative ZO phonon mode could be removed by the selection of an appropriate substrate, see [3,8]. The ability of potentials for 3D silicon to reproduce 2D silicon is poorly studied. There are several papers where the quality of potentials for 3D silicon has been assessed, see e.g. [9-11] but not for silicene. The intention of this work is first to determine the structural and mechanical properties of 2D silicon using first-principles method and then to test the ability of different interatomic potentials to reproduce these properties.

2 Methods

Analyzing the available literature concerning all phases of single-layer (SL) Si, it is not feasible to find all structural, mechanical and phonon data obtained in one consistent way. The availability of experimental data is actually limited to the silicene grown on some support, a pristine free-standing SL sheet of silicene has not been discovered to date [4,12], and therefore we must use *ab initio* calculations. Unfortunately, also *ab initio* calculations, most often DFT, differ in the calculation methodology, i.e., they use different functional bases, different pseudopotentials or exchange-correlation (XC) functionals, and parameters such as cohesive energy and elastic constants are poorly accessible. For this reason, structural and mechanical data, i.e., lattice parameters, average cohesive energy, average bond length, average height, 2D elastic constants as well as phonon data are determined here using a single consistent first-principles approach as described in the next

Section 2.1. These data were further considered as reference data and marked as Value^{DFT}. Then the same data were determined, as described in Section 2.2 using the analyzed molecular potentials from Subsection 2.2.1 and are marked as Value^{potential}. Having both data, we can simply define mean absolute percentage error (MAPE):

$$\text{MAPE} = \frac{100\%}{n} \sum_{t=1}^n \frac{|\text{Value}^{\text{DFT}} - \text{Value}^{\text{potential}}|}{\text{Value}^{\text{DFT}}}, \quad (1)$$

that will allow us to quantify the potentials under examination.

For 2D materials, directional 2D Young's moduli

$$E_{[10]}^{2D} = \frac{C_{11}C_{22} - C_{12}^2}{C_{22}} \quad \text{and} \quad E_{[01]}^{2D} = \frac{C_{11}C_{22} - C_{12}^2}{C_{11}}, \quad (2)$$

2D Poisson's ratios

$$\nu_{[10]}^{2D} = \frac{C_{12}}{C_{22}} \quad \text{and} \quad \nu_{[01]}^{2D} = \frac{C_{12}}{C_{11}}, \quad (3)$$

and the 2D shear modulus

$$G_{33}^{2D} = C_{33}, \quad (4)$$

are often used instead of elastic constants C_{ij} . Due to symmetry for hexagonal lattices, this reduces to one 2D Young's modulus E and a one 2D Poisson's ratio, see [13].

2.1 *AB INITIO* Calculations

The *ab initio* calculation methodology here is closely analogous to that used in [14], i.e., the density functional theory (DFT) [15,16], ABINIT plane-wave approximation code [17,18], local density approximation (LDA) [19,20] as an exchange-correlation (XC) functional, optimized norm-conserving Vanderbilt pseudopotential [21] (ONCVPP). The *cut-off* energy and the electron configuration for Si used in the DFT calculations according to the pseudopotential and Gaussian

smearing scheme with $tsmear$ (Ha)=0.02 were used. To generate K-Points grids $kptrlen$ was set to 43.0. Since 2D structures were analyzed in the z-direction, a vacuum of 20 Å was applied. The initial data for the five structures analyzed were deduced from [6] and [7]. The structures were then carefully relaxed with full optimization of cell geometry and atomic coordinates [14].

The average cohesive energy E_c (eV/atom) was computed as the difference in the total energy of a given relaxed earlier structure and its individual atoms placed in a cubic box of sufficient size. The theoretical ground state, T=0 K, elastic constants, C_{ij} , of all the previously optimized structures were computed using the metric tensor formulation of strain in density functional perturbation theory (DFPT) [22]. The mechanical stability of the analyzed structures was verified by calculating the so-called Kelvin moduli [23-25]. To calculate the phonons, the density functional perturbation theory implemented in ABINIT [17,18] was employed. The phonon dispersion curves along the path $\Gamma[0,0,0]$ - $M[1/2,0,0]$ - $K[1/3,1/3,0]$ - $\Gamma[0,0,0]$ [26] of the analyzed structures were then used to identify their dynamical stability [27], complementary to the mechanical stability.

2.2 Molecular Calculations

To perform molecular calculations the molecular statics (MS) method, T=0 K, [28-30] was used by means of the Large-scale Atomic/Molecular Massively Parallel Simulator (LAMMPS) [31] and analyzed by means of the Open Visualization Tool (OVITO) [32]. As for DFT calculations, the structures were here fully pre-relaxed with the conjugate gradient (CG) algorithm and then the elastic constants, C_{ij} , were calculated for them using the stress-strain method with the maximum strain magnitude set to 10^{-6} [30,31]. In the z-direction, a vacuum was set to 20 Å.

To measure performance of the interatomic potentials analyzed, the series of molecular dynamics (MD) simulations (200 atoms and 10000 timesteps, NVT ensemble) and LAMMPS's built-in function *timesteps/s* were used. The results were then normalized relative to the longest run time.

2.2.1 Interatomic Potentials

The parameterizations of the potentials listed below were obtained from

the NIST Interatomic Potentials Repository and/or from LAMMPS code sources.

1. **Tersoff1988** [33]: the original Tersoff potential for silicon (it is important to remember that this paper proposed a form of potential rather than a specific parametrization for silicon)
2. **Tersoff2007** [34]: the Tersoff potential fitted to the elastic constants of diamond silicon
3. **Tersoff2017** [35]: newer, better optimized the Tersoff potential for silicon
4. **MEAM2007** [36]: a semi-empirical interatomic potential for silicon based on the modified embedded atom method (MEAM) formalism
5. **MEAM2011** [37]: spline-based modified embedded-atom method (MEAM) potential for Si fitted for silicon interstitials
6. **SW1985** [38]: the Stillinger–Weber (SW) potential fitted to solid and liquid forms of Si
7. **SW2014** [39]: the Stillinger–Weber (SW) potential fitted to phonon dispersion curves of a single-layer Si sheet
8. **EDIP** [40]: the environment-dependent interatomic potential (EDIP) fitted to various bulk phases and defect structures of Si
9. **ReaxFF** [41]: the reactive force-field (ReaxFF) fitted to a training set of DFT data that pertain to Si/Ge/H bonding environments
10. **COMB** [42]: the charge optimized many-body (COMB) potential fitted to a pure silicon and five polymorphs of silicon dioxide
11. **SNAP** [43]: the machine-learning-based (ML-IAP) linear variant of spectral neighbor analysis potential (SNAP) fitted to total energies and interatomic forces in ground-state Si, strained structures and slab structures obtained from DFT calculations

12. **qSNAP** [43]: the machine-learning-based (ML-IAP) quadratic variant of spectral neighbor analysis potential (qSNAP) fitted to total energies and interatomic forces in ground-state Si, strained structures and slab structures obtained from DFT calculations
13. **SO(3)** [44]: the machine-learning-based (ML-IAP) variant of the SO(3) smooth power spectrum potential (SO(3)) fitted to the ground-state of the crystalline silicon structure, strained structures, slabs, vacancy, and liquid configurations from DFT simulations
14. **ACE** [45]: the machine-learning-based (ML-IAP) variant of the atomic cluster expansion potential (ACE) fitted to a wide range of properties of 3D silicon determined from the DFT calculation

3 Results and Discussion

3.1 Structural and Mechanical Properties

Basic cells for the five silicene polymorphs, i.e, the flat (FS):(hP2, P6/mmm, no.191), low-buckled (LBS):(hP2, P-3m1, no.164), trigonal dumbbell (TDS):(hP7, P-62m, no.189), honeycomb dumb-bell (HDS):(hP8, P6/mmm, no.191) and large honeycomb dumbbell (LHDS):(hP10, P6/mmm, no.191) are depicted in Figure 1 and additionally the crystallographic data for them are stored in Crystallographic Information Files (CIFs) in the Supporting Information.

The results of first-principles calculations show that all the silicene phases have hexagonal symmetry. The symmetry characteristic of a structure determines the symmetry of its physical properties (*Neumann's Principle* and *Curie laws*) [46,47]. For 2D linear hyperelastic materials, there are four classes of symmetry [24] and hexagonal symmetry implies isotropy of the stiffness tensor, i.e., there are only two distinct elastic constants and they satisfy, in Voigt notation, such conditions that $C_{11} = C_{22}$, $C_{33} = (C_{11} - C_{12})/2$.

Determined from DFT computations structural and mechanical characteristics, namely lattice parameters, average cohesive energy, average bond length, average height, 2D elastic constants, 2D Young's modulus, Poisson's ratio and 2D Kelvin moduli, of the five silicene polymorphs analyzed

are gathered in Table 1. Since we are analyzing free-standing silicene here, which has not yet been observed in experiments, we compare the results of the calculations with those of other authors. We find that the lattice constants, average bond length, average height and cohesive energy agree at the DFT level of accuracy with other calculations. Mechanical properties of silicene are available in the literature only for the LBS phase and are limited to 2D Young's modulus and Poisson's ratio only. These quantities are also in reasonable agreement with the present results. It is immediately worth noting that all the calculated 2D Kelvin moduli for all silicene phases are positive, which results in mechanical stability [24]. The phonon spectra along the Γ -**M**-**K**- Γ path for the five silicene polymorphs is depicted in Figure 2. The analysis of the computed curves shows that the phases TDS, LBS, HDS and LHDS are not only mechanically but also dynamically stable, i.e., all phonon modes have positive frequencies anywhere. The FS phase is mechanically stable, but can be dynamically unstable, i.e., optical ZO phonon mode has a negative frequency. Other authors have also observed similar FS phase behavior [4,12], however, but since silicene is not a free-standing structure in nature the selection of a proper substrate may dampen the out-of-plane vibration mode and a flat silicene may be produced [3]. So it was decided that this phase was also included in the molecular calculations.

3.2 Performance of Interatomic Potentials

The computed with the use of molecular statics and the fourteen various interatomic potentials for silicon (**Tersoff** (×3), **MEAM** (×2), **Stillinger-Weber** (×2), **EDIP**, **ReaxFF**, **COMB** and machine-learning-based (**ML-IAP** (×4)), enumerated in Section 2.2.1, twelve structural and mechanical properties, i.e., lattice parameters a , b , average cohesive energy, average bond length, average height h , 2D elastic constants C_{ij} , 2D Kelvin moduli of the flat silicene (FS) phase are collected in Table 2, of the low-buckled silicene (LBS) in Table 3, of the trigonal dumbbell silicene (TDS) in Table 4, of the honeycomb dumbbell silicene (HDS) in Table 5 and of the large honeycomb dumbbell silicene (LHDS) in Table 6, respectively. The aforementioned results, for each of the five silicene phases, were then compared with those from the DFT calculations using the mean absolute

percentage error (MAPE) defined in Equation 1. Let's briefly analyze the results for each phase, and so for the FS phase the most accurate is the **MEAM2011** potential, it has the lowest MAPE, see Table 2, for the LBS phase the **Tersoff2107**, see Table 3, for the TDS phase the **ReaxFF**, see Table 4, for the HDS the **ReaxFF**, see Table 5 and for the LHDS again the **ReaxFF** potential, see Table 6, respectively. Now let's take a summary look. Seven of the fourteen potentials analyzed, namely **Tersoff2007**, **Tersoff2017**, **SW1985**, **SW2014**, **ReaxFF**, **SNAP** and **ACE**, are able to correctly reproduce the structural properties of the five polymorphs of silicene, see Tabs. 3, 5, 6. Two potentials: **ReaxFF** and **MEAM2011** give the best quantitative performance measured by the total mean absolute percentage error (MAPE), see Tab. 6. From the point of view of the cost of calculations in terms of relative performance measured as normalized timesteps/second in molecular dynamics (MD) simulation the **EDIP** and **Stillinger-Weber** potentials are the fastest, about 5 times faster than the **MEAM** and **Tersoff** potentials, about 100 times faster than **ReaxFF** and **COMB**, and up to 2000 times faster than the **ML-IAP(ACE)** potential, see Tab. 6. It is also worth noting, that the machine-learning-based (**ML-IAP**) interatomic potentials, according to the methodology used, are not superior to classical potentials in terms of performance (MAPE) and are instead even three orders of magnitude more computationally expensive, see Tab. 6.

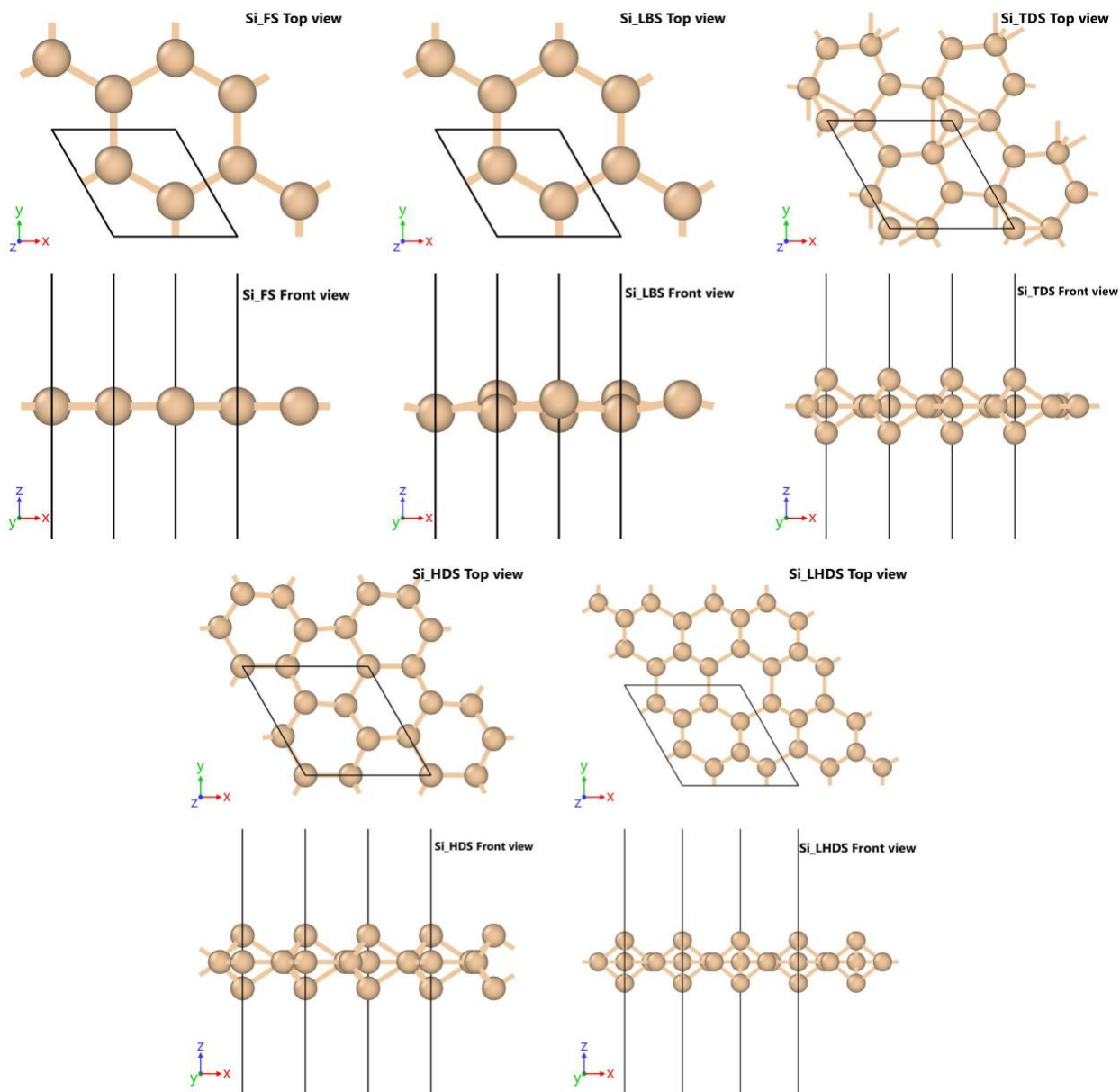


Figure 1: Polymorphs of silicene.

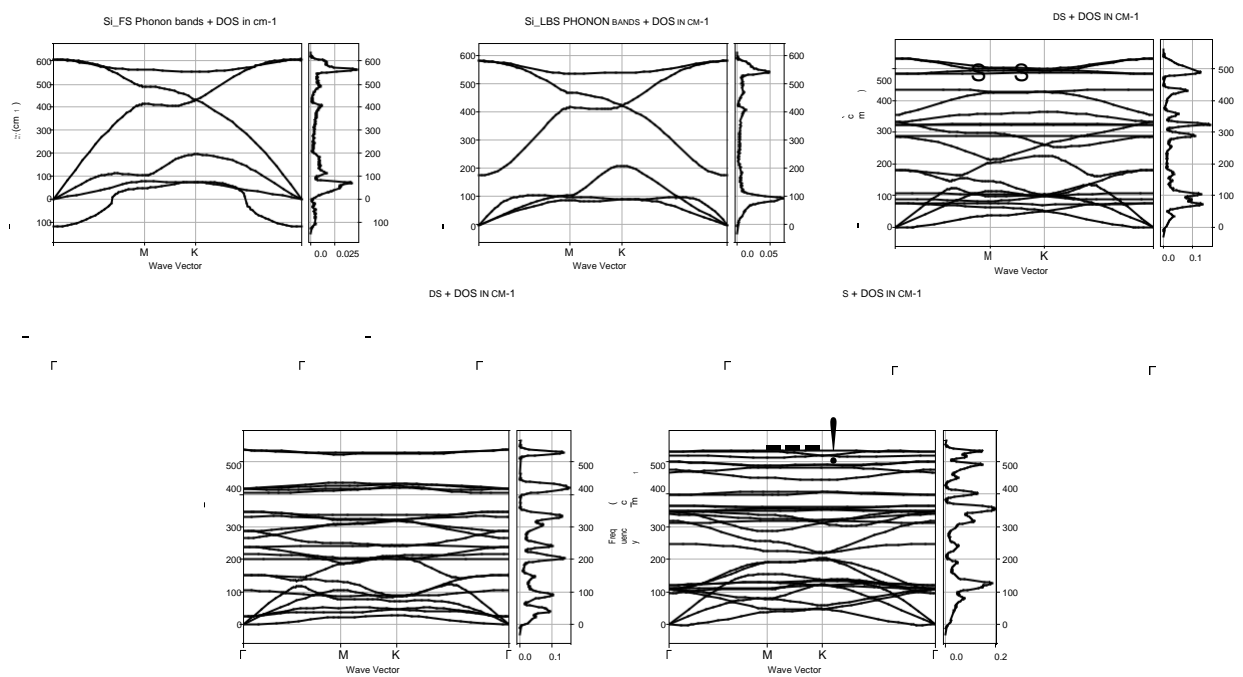


Figure 2: Phonon dispersion and density of states (DOS) of the flat (FS), low-buckled (LBS), trigonal dumbbell (TDS), honeycomb dumbbell (HDS) and large honeycomb dumbbell (LHDS) single-layer silicon (silicene) phases. High symmetry points: $\Gamma[0,0,0]$, $M[1/2,0,0]$, $K[1/3,1/3,0]$.

Table 1: Structural and mechanical properties of flat (FS), low-buckled (LBS), trigonal dumbbell (TDS), honeycomb dumbbell (HDS) and large honeycomb dumbbell (LHDS) silicene phases from density functional theory (DFT) calculations: lattice parameters a, b (Å), average cohesive energy (eV/atom), average bond length (Å), average height h (Å), 2D elastic constants C_{ij} (N/m), 2D Young's modulus E (N/m), Poisson's ratio and 2D Kelvin moduli (N/m).

Polymorph	FS		LBS		TDS		HDS		LHDS	
Source	This work	Refs.	This work	Refs.	This work	Refs.	This work	Refs.	This work	Refs.
a	3.855	3.90 ^a	3.828	3.87 ^a , 3.83 ^b	6.434	6.52 ^b	6.297	6.38 ^b	7.334	7.425 ^b
b	3.855	3.90 ^a	3.828	3.87 ^a , 3.83 ^b	6.434	6.52 ^b	6.297	6.38 ^b	7.334	7.425 ^b
–	4.562	4.764 ^a	4.577	4.784 ^a , 5.16 ^b	4.679		4.679		4.769	
†	2.225		2.249	2.25 ^b	2.331		2.399		2.357	
h	0.0	0.0 ^a	0.421 ^a	0.45 ^a , 0.44 ^b	2.734		2.635		2.683	
C_{11}	84.8		69.2		100.5		141.6		104.5	
C_{22}	84.8		69.2		100.5		141.6		104.5	
C_{12}	40.6		22.1		52.3		96.4		52.7	
C_{33}	22.1		23.6		24.1		22.6		25.9	
E	65.4		62.2	61.8 ^a	73.3		76.0		77.9	
	0.48		0.32	0.31 ^a	0.52		0.68		0.50	
	125.4		91.3		152.8		238.0		157.2	
	44.3		47.1		48.3		45.2		51.8	
	44.3		47.1		48.3		45.2		51.8	

^aRef. [48], ^b Ref. [7].

† An average bond lengths calculated using radial pair distribution function with a *cut-off* radius = 3.0 Å and a number of histogram bins = 1000 [32].

Table 2: Structural and mechanical properties of flat silicene (FS) from molecular calculations: lattice parameters a, b (Å), average cohesive energy (eV/atom), average bond length (Å), average height h (Å), 2D elastic constants C_{ij} (N/m), 2D Kelvin moduli (N/m), mean absolute percentage error (MAPE) (%).

Method	DFT	Tersoff 1988	Tersoff 2007	Tersoff 2017	MEAM 2007	MEAM 2011	SW 1985	SW 2014	EDIP	ReaxFF	COMB	ML-IAP SNAP	ML-IAP qSNAP	ML-IAPML-IAP SO(3)	ML-IAP ACE
a	3.855	4.008	4.019	4.042	4.457	3.960	4.104	3.886	4.018	3.950	3.990	4.121	4.019	4.051	3.850
b	3.855	4.008	4.019	4.042	4.457	3.960	4.104	3.886	4.018	3.950	3.990	4.121	4.019	4.051	3.850
h	4.562	3.926	3.828	3.687	3.288	3.793	3.145	2.564	4.010	3.408	3.911	4.575	4.499	4.407	0.962
C_{11}	2.225	2.315	2.321	2.333	2.573	2.288	2.369	2.243	2.321	2.282	2.306	2.381	2.321	2.340	2.222
C_{22}	0.0	0.0	0.0	0.0	0.0	0.0	0.0	0.0	0.0	0.0	0.0	0.0	0.0	0.0	0.0
C_{33}	84.8	54.6	55.2	47.7	57.3	84.0	58.8	57.3	87.4	74.7	79.7	41.5	24.7	41.0	88.9
C_{12}	84.8	54.6	55.2	47.7	57.3	84.0	58.8	57.3	87.4	74.7	79.7	41.5	24.7	41.0	88.9
C_{13}	40.6	49.5	47.4	52.8	29.7	40.8	34.4	33.0	9.2	36.8	23.9	16.2	17.6	23.9	44.8
C_{23}	22.1	2.6	3.9	-2.6	13.8	21.6	12.2	12.2	39.1	19.0	27.9	12.6	3.5	8.6	22.0
C_{33}	125.4	104.0	102.6	100.5	87.0	124.8	93.2	90.3	96.6	111.5	103.6	57.6	42.3	64.9	133.7
C_{11}	44.3	5.1	7.8	-5.1	27.6	43.3	24.4	24.4	78.2	37.9	55.8	25.3	7.0	17.1	44.1
C_{12}	44.3	5.1	7.8	-5.1	27.6	43.3	24.4	24.4	78.2	37.9	55.8	25.3	7.0	17.1	44.1
MAPEFS		36.515	34.619	45.987	28.174	3.147	26.093	26.595	32.827	10.904	15.805	33.284	48.283	35.946	9.757

Table 3: Structural and mechanical properties of low-buckled silicene (LBS) from molecular calculations: lattice parameters a, b (Å), average cohesive energy (eV/atom), average bond length (Å), average height h (Å), 2D elastic constants C_{ij} (N/m), 2D Kelvin moduli (N/m), mean absolute percentage error (MAPE) (%).

Method	DFT	Tersoff 1988	Tersoff 2007	Tersoff 2017	MEAM 2007	MEAM 2011	SW 1985	SW 2014	EDIP	ReaxFF	COMB	ML-IAP SNAP	ML-IAPML-IAP qSNAP	ML-IAPML-IAP SO(3)	ML-IAP ACE
a	3.828	3.309	3.820	3.870	4.150	3.837	3.840	3.812	4.018	3.843	3.990	3.916	3.808	3.743	3.702
b	3.828	3.309	3.820	3.870	4.150	3.837	3.840	3.812	4.018	3.843	3.990	3.916	3.808	3.743	3.702
h	4.577	3.936	3.936	3.755	3.404	3.851	3.252	2.572	4.010	3.454	3.911	4.648	4.624	4.606	0.926
C_{11}	2.249	2.315	2.312	2.315	2.534	2.297	2.351	2.243	2.321	2.300	2.306	2.390	2.366	2.347	2.242
C_{22}	0.421	1.304	0.690	0.327	0.820	0.608	0.784	0.427	0.0 [‡]	0.610	0.0 [‡]	0.774	0.859	0.913	0.675
C_{33}	69.2	0.006	59.6	50.1	38.4	47.1	36.4	30.8	87.4	49.0	79.7	24.8	28.8	31.7	55.0
C_{12}	69.2	0.006	59.6	50.1	38.4	47.1	36.4	30.8	87.4	49.0	79.7	24.8	28.8	31.7	55.0
C_{13}	22.1	0.002	4.1	5.5	4.4	10.6	6.1	5.4	9.2	14.1	23.9	5.6	6.3	9.0	2.7
C_{23}	23.6	0.002	27.7	22.3	17.0	18.3	15.1	12.7	39.1	17.5	27.9	9.6	11.2	11.4	26.1
C_{33}	91.3	0.008	63.7	55.7	42.7	57.7	42.6	36.2	96.6	63.1	103.6	30.4	35.1	40.6	57.7
C_{11}	47.1	0.004	55.5	44.6	34.0	36.5	30.3	25.5	78.2	34.9	55.8	19.2	22.4	22.7	52.3
C_{12}	47.1	0.004	55.5	44.6	34.0	36.5	30.3	25.5	78.2	34.9	55.8	19.2	22.4	22.7	52.3
MAPELBS		79.467	22.781	19.235	37.991	23.569	37.306	35.911	36.630	22.977	19.433	45.306	43.176	42.060	28.792

[‡] Input LBS converges to FS.

Table 4: Structural and mechanical properties of trigonal dumbbell silicene (TDS) from molecular calculations: lattice parameters a, b (Å), average cohesive energy (eV/atom), average bond length (Å), average height h (Å), 2D elastic constants C_{ij} (N/m), 2D Kelvin moduli (N/m), mean absolute percentage error (MAPE) (%).

Method	DFT	Tersoff 1988	Tersoff 2007	Tersoff 2017	MEAM 2007	MEAM 2011	SW 1985	SW 2014	EDIP	ReaxFF	COMB	ML-IAP SNAP	ML-IAPML-IAP qSNAP	ML-IAPML-IAP SO(3)	ML-IAP ACE
a	6.434	6.480	6.471	6.475	7.140	6.511	6.600	6.291	6.759	6.380	6.574	6.777	6.797	6.518	6.448
b	6.434	6.480	6.471	6.475	7.140	6.511	6.600	6.291	6.759	6.380	6.574	6.777	6.797	6.518	6.448
h	4.679	4.248	3.865	3.890	3.427	3.865	3.322	2.591	4.075	3.551	3.723	4.726	4.693	4.607	0.4606
C_{11}	2.331	2.362	2.371	2.362	2.590	2.376	2.431	2.315	2.416	2.344	2.387	2.398	2.404	2.505	2.429
C_{22}	2.734	2.870	3.110	3.056	3.228	2.856	3.260	3.100	2.628	3.115	2.994	2.518	2.540	3.058	2.649
C_{33}	100.5	79.4	67.9	51.4	69.9	80.5	78.7	68.4	60.3	94.6	70.8	44.9	36.7	35.3	90.5
C_{12}	100.5	79.4	67.9	51.4	69.9	80.5	78.7	68.4	60.3	94.6	70.8	44.9	36.7	35.3	90.5
C_{13}	52.3	63.2	39.4	39.0	34.9	31.0	39.6	35.1	30.2	39.7	25.6	16.1	16.7	10.2	33.0
C_{23}	24.1	8.1	14.3	6.2	17.5	24.8	19.6	16.7	15.1	27.4	22.6	14.4	10.0	12.5	28.8
C_{33}	152.8	142.7	107.3	90.5	104.8	111.5	118.2	103.5	90.5	134.3	96.4	61.1	53.4	45.5	123.5
C_{11}	48.3	16.2	28.5	12.4	35.0	49.5	39.1	33.3	30.1	54.9	45.2	28.8	20.1	25.0	57.6
C_{12}	48.3	16.2	28.5	12.4	35.0	49.5	39.1	33.3	30.1	54.9	45.2	28.8	20.1	25.0	57.6
MAPETDS		23.790	22.993	34.815	23.821	11.809	17.077	23.723	25.537	10.755	16.881	31.929	38.100	37.357	19.317

Table 5: Structural and mechanical properties of honeycomb dumbbell silicene (HDS) from molecular calculations: lattice parameters a, b (Å), average cohesive energy (eV/atom), average bond length (Å), average height h (Å), 2D elastic constants C_{ij} (N/m), 2D Kelvin moduli (N/m), mean absolute percentage error (MAPE) (%).

Method	DFT	Tersoff 1988	Tersoff 2007	Tersoff 2017	MEAM 2007	MEAM 2011	SW 1985	SW 2014	EDIP	ReaxFF	COMB	ML-IAP SNAP	ML-IAPML-IAP qSNAP	ML-IAP SO(3)	ML-IAP ACE
a	6.297	6.074 [†]	6.133	6.114	5.608 [†]	6.364 [†]	6.272	6.063	6.349 [†]	6.048	6.344	6.644	6.510 [†]	5.030 [†]	6.250
b	6.297	5.864 [†]	6.133	6.114	6.127 [†]	6.279 [†]	6.272	6.063	6.389 [†]	6.048	6.344	6.644	6.344 [†]	5.818 [†]	6.250
$-$	4.679	4.334	3.738	3.816	3.663	4.008	3.243	2.467	4.105	3.366	3.481	4.766	4.699	4.873	0.391
h	2.399	2.398	2.425	2.408	2.641	2.405	2.495	2.394	2.489	2.396	2.511	2.436	2.457	2.612	2.371
C_{11}	2.635	2.596	3.050	3.006	3.500	2.990	3.189	3.010	2.365	2.952	2.989	2.404	2.438	2.162	2.559
C_{22}	141.6	89.3	59.4	64.0	56.2	78.2	57.4	35.6	78.0	75.4	14.3	41.9	30.8	76.5	69.6
C_{12}	141.6	46.3	59.4	64.0	57.1	82.4	57.4	35.6	45.5	75.4	14.3	41.9	16.0	73.0	69.6
C_{33}	96.4	20.4	24.6	31.3	17.3	7.1	25.3	14.9	46.3	31.4	-37.4	16.2	13.8	-10.2	10.6
	22.6	24.8	17.4	16.3	16.7	26.2	16.0	10.4	9.6	22.0	25.8	12.9	11.7	2.7	29.5
	238.0	102.1	84.0	95.3	76.6	87.8	82.7	50.6	119.7	106.8	51.7	58.1	41.2	84.9	80.1
	45.2	57.7	34.8	32.7	44.5	72.9	32.0	20.7	13.6	43.9	-23.1 [*]	25.7	24.3	64.7	59.0
	45.2	25.5	34.8	32.7	-1.2 [*]	52.3	32.0	20.7	9.2	43.9	51.7	25.7	23.4	5.5	59.0
MAPE _{HDS}		28.361	30.540	29.931	39.880	30.392	33.503	45.400	37.500	22.740	51.780	37.684	41.062	45.571	37.134

[†] Potential does not reproduce the correct symmetry of the structure ($a \neq b$),

^{*} Negative Kelvin moduli indicating a lack of mechanical stability.

Table 6: Structural and mechanical properties of large honeycomb dumbbell silicene (LHDS) from molecular calculations: lattice parameters a, b (Å), average cohesive energy (eV/atom), average bond length (Å), average height h (Å), 2D elastic constants C_{ij} (N/m), 2D Kelvin moduli (N/m), mean absolute percentage error (MAPE) (%), relative performance measured as normalized timesteps/second in molecular dynamics (MD) simulation.

Method	DFT	Tersoff 1988	Tersoff 2007	Tersoff 2017	MEAM 2007	MEAM 2011	SW 1985	SW 2014	EDIP	ReaxFF	COMB	ML-IAPML-IAP SNAP	ML-IAPML-IAP qSNAP	ML-IAP SO(3)	ML-IAP ACE
a	7.334	7.000 [†]	7.249	7.236	7.900 [†]	7.363	7.403	7.062	7.705	7.167	7.422	7.648	7.741	7.427	7.393
b	7.334	6.978 [†]	7.249	7.236	7.560 [†]	7.363	7.403	7.062	7.705	7.167	7.422	7.648	7.741	7.427	7.393
$-$	4.769	4.468	3.897	4.004	3.505	3.911	3.399	2.602	4.113	3.623	3.646	4.804	4.794	4.698	0.370
h	2.357	2.381	2.387	2.369	2.627	2.407	2.456	2.345	2.438	2.370	2.454	2.436	2.403	2.385	2.515
C_{11}	2.683	2.692	3.109	3.050	3.050	2.857	3.250	3.100	2.637	3.112	2.994	2.538	2.562	2.700	2.712
C_{22}	104.5	2.3	78.5	68.6	45.6	88.0	84.5	73.0	53.7	99.0	53.1	44.6	43.8	25.9	59.8
C_{12}	104.5	7.3	78.5	68.6	56.2	88.0	84.5	73.0	53.7	99.0	53.1	44.6	43.8	25.9	59.8
C_{33}	52.7	-13.1	42.3	25.5	22.0	29.9	46.1	38.9	36.0	40.4	31.7	16.1	19.1	0.4	15.2
	25.9	9.0	18.1	21.6	14.0	29.0	19.2	17.1	8.8	29.3	10.7	14.2	12.3	12.7	22.3
	157.2	18.5	120.8	94.1	73.6	117.9	130.6	111.9	89.7	139.4	84.8	60.6	62.8	26.4	75.0
	51.8	17.8	36.2	43.1	28.8	58.1	38.4	34.1	17.6	58.6	21.5	28.5	24.7	25.5	44.7
	51.8	-8.5 [*]	36.2	43.1	27.4	58.1	38.4	34.1	17.6	58.6	21.5	28.5	24.7	25.5	44.7
MAPE _{LHDS}		55.693	18.373	20.287	34.499	13.636	16.741	23.855	33.228	10.809	33.466	33.219	34.603	40.928	29.310
MAPE		223.826	129.306	150.256	164.364	82.553	130.721	155.483	165.722	78.185	137.365	181.422	205.224	201.861	124.310
timesteps/s		387.2	382.7	355.2	505.7	416.9	904.9	1753.8	2032.1	23.6	26.4	7.9	4.7	4.2	1.0

[†] Potential does not reproduce the correct symmetry of the structure ($a \neq b$),

^{*} Negative Kelvin moduli indicating a lack of mechanical stability.

4 Conclusion

A systematic quantitative comparative study of various silicon interatomic potentials for reproducing the properties of five silicene (2D silicon) polymorphs was shown. In order to compare the fourteen potentials listed in Section 2.2.1, the structural and mechanical properties of flat (FS), low-buckled (LBS), trigonal dumbbell (TDS), honeycomb dumbbell (HDS) and large honeycomb dumbbell (LHDS) silicene (Fig. 1) obtained from the density functional theory (DFT) and molecular statics (MS) computations were used. The computational cost, the performance, of the analyzed potentials were also compared. It can be stated that considering the performance and the cost of calculations, the classical potentials of Tersoff, SW and MEAM type seem to be the best choice here. Although data for silicene polytypes were not used in the optimization of these potentials, they were able to reproduce their properties well. There is a consequence that they are based on physics, have a natural extrapolation ability, and not just interpolate data. I hope that the findings done here will help other researchers in selecting the suitable potentials for their purposes and will be a hint to parameterize new potentials for silicene.

Supporting Information

Crystallographic Information Files (CIF) for polymorphs of silicene.

Supporting Information File 1:

File Name: Si_FS.cif

File Format: CIF

Title: flat silicene (FS)

Supporting Information File 2:

File Name: Si_LBS.cif

File Format: CIF

Title: low-buckled silicene (LBS)

Supporting Information File 3:

File Name: Si_TDS.cif

File Format: CIF

Title: trigonal dumbbell silicene (TDS)

Supporting Information File 4:

File Name: Si_HDS.cif

File Format: CIF

Title: honeycomb dumbbell silicene (HDS)

Supporting Information File 5:

File Name: Si_LHDS.cif

File Format: CIF

Title: large honeycomb dumbbell silicene (LHDS)

Si_FS.cif -- in P1.1 -- non-magnetic

data_Si_FS_191

_audit_creation_date

222-8-4

_audit_creation_method "Bilbao Crystallographic Server"
_symmetry_Int_Tables_number 1
#_symmetry_space_group_name_H-M "P11"
_cell_length_a 3.85481
_cell_length_b 3.85481
_cell_length_c 2.
_cell_angle_alpha 9.
_cell_angle_beta 9.
_cell_angle_gamma 12.

loop_

_symmetry_equiv_pos_site_id
_symmetry_equiv_pos_as_xyz
1 x,y,z

loop_

_atom_site_label
_atom_site_type_symbol
_atom_site_fract_x
_atom_site_fract_y
_atom_site_fract_z
_atom_site_occupancy
Si1 Si .33333 .66667 .5 1.
Si2 Si .66666 .33333 .5 1.

Si_LBS.cif -- in P1.1 -- non-magnetic

data_Si_LBS_164

```

_audit_creation_date          222-8-4
_audit_creation_method       "Bilbao Crystallographic Server"
_symmetry_Int_Tables_number  1
#_symmetry_space_group_name_H-M "P11"
_cell_length_a               3.82781
_cell_length_b               3.82781
_cell_length_c               2.
_cell_angle_alpha            9.
_cell_angle_beta             9.
_cell_angle_gamma            12.

```

loop_

```

_symmetry_equiv_pos_site_id
_symmetry_equiv_pos_as_xyz
  1  x,y,z

```

loop_

```

_atom_site_label
_atom_site_type_symbol
_atom_site_fract_x
_atom_site_fract_y
_atom_site_fract_z
_atom_site_occupancy
Si1 Si .33333 .66667 .48915 1.
Si2 Si .66666 .33333 .5185 1.

```

```
# Si_TDS.cif -- in P1.1 -- non-magnetic
```

```

data_Si_TDS_189
_audit_creation_date          222-8-4
_audit_creation_method        "Bilbao Crystallographic Server"
_symmetry_Int_Tables_number   1
#_symmetry_space_group_name_H-M "P11"
_cell_length_a                6.43381
_cell_length_b                6.43381
_cell_length_c                2.
_cell_angle_alpha             9.
_cell_angle_beta              9.
_cell_angle_gamma             12.

```

loop_

```

_symmetry_equiv_pos_site_id
_symmetry_equiv_pos_as_xyz
  1  x,y,z

```

loop_

```

_atom_site_label
_atom_site_type_symbol
_atom_site_fract_x
_atom_site_fract_y
_atom_site_fract_z
_atom_site_occupancy
Si1 Si .33333 .66667 .5 1.
Si2 Si .66666 .33333 .5 1.
Si3 Si .29982 . .5 1.

```

Si4 Si . .29982 .5 1.

Si5 Si .718 .718 .5 1.

Si6 Si . . .4322 1.

Si7 Si . . .56798 1.

Si_HDS.cif -- in P1.1 -- non-magnetic

data_Si_HDS_189

_audit_creation_date	222-8-4
_audit_creation_method	"Bilbao Crystallographic Server"
_symmetry_Int_Tables_number	1
#_symmetry_space_group_name_H-M	"P11"
_cell_length_a	6.29732
_cell_length_b	6.29732
_cell_length_c	2.
_cell_angle_alpha	9.
_cell_angle_beta	9.
_cell_angle_gamma	12.

loop_

_symmetry_equiv_pos_site_id	
_symmetry_equiv_pos_as_xyz	
1	x,y,z

loop_

_atom_site_label	
_atom_site_type_symbol	
_atom_site_fract_x	

```

_atom_site_fract_y
_atom_site_fract_z
_atom_site_occupancy
Si1 Si . . .5 1.
Si2 Si .35934 . .5 1.
Si3 Si . .35934 .5 1.
Si4 Si .6466 .6466 .5 1.
Si5 Si .33333 .66667 .56577 1.
Si6 Si .66666 .33333 .43423 1.
Si7 Si .33334 .66667 .43423 1.
Si8 Si .66667 .33334 .56577 1.

```

```
# Si_LHDS.cif -- in P1.1 -- non-magnetic
```

```
data_Si_LHDS_191
```

```

_audit_creation_date          222-8-4
_audit_creation_method        "Bilbao Crystallographic Server"
_symmetry_Int_Tables_number   1
#_symmetry_space_group_name_H-M "P11"
_cell_length_a                7.33381
_cell_length_b                7.33381
_cell_length_c                2.
_cell_angle_alpha             9.
_cell_angle_beta              9.
_cell_angle_gamma             12.

```

```
loop_
```

```
_symmetry_equiv_pos_site_id
```

_symmetry_equiv_pos_as_xyz

1 x,y,z

loop_

_atom_site_label

_atom_site_type_symbol

_atom_site_fract_x

_atom_site_fract_y

_atom_site_fract_z

_atom_site_occupancy

Si1 Si .18192 .36384 .5 1.

Si2 Si .8188 .18192 .5 1.

Si3 Si .63616 .8188 .5 1.

Si4 Si .8188 .63616 .5 1.

Si5 Si .18192 .8188 .5 1.

Si6 Si .36384 .18192 .5 1.

Si7 Si .33333 .66667 .43292 1.

Si8 Si .66666 .33333 .43292 1.

Si9 Si .66666 .33333 .5678 1.

Si1 Si .33333 .66666 .5678 1.

Acknowledgements

Additional assistance was granted through the computing cluster GRAFEN at Biocentrum Ochota, the Interdisciplinary Centre for Mathematical and Computational Modelling of Warsaw University (ICM UW) and Poznań Supercomputing and Networking Center (PSNC).

Funding

This work was supported by the National Science Centre (NCN – Poland) Research Project: No. 2021/43/B/ST8/03207.

References

1. Akinwande, D.; Brennan, C. J.; Bunch, J. S.; Egberts, P.; Felts, J. R.; Gao, H.; Huang, R.; Kim, J.-S.; Li, T.; Li, Y.; Liechti, K. M.; Lu, N.; Park, H. S.; Reed, E. J.; Wang, P.; Yakobson, B. I.; Zhang, T.; Zhang, Y.-W.; Zhou, Y.; Zhu, Y. *Extreme Mechanics Letters* **2017**, *13*, 42–77. doi:10.1016/j.eml.2017.01.008.
2. Lei, Y.; Zhang, T.; Lin, Y.-C.; Granzier-Nakajima, T.; Bepete, G.; Kowalczyk, D. A.; Lin, Z.; Zhou, D.; Schranghamer, T. F.; Dodda, A.; Sebastian, A.; Chen, Y.; Liu, Y.; Pour-tois, G.; Kempa, T. J.; Schuler, B.; Edmonds, M. T.; Quek, S. Y.; Wurstbauer, U.; Wu, S. M.; Glavin, N. R.; Das, S.; Dash, S. P.; Redwing, J. M.; Robinson, J. A.; Terrones, M. *ACS Nanoscience Au* **2022**, *2* (6), 450–485. doi:10.1021/acsnanoscienceau.2c00017.
3. Roome, N. J.; Carey, J. D. *ACS Applied Materials & Interfaces* **2014**, *6* (10), 7743–7750. doi:10.1021/am501022x.
4. Spencer, M.; Morishita, T. *Silicene: Structure, Properties and Applications*; Springer Cham, 2016; Vol. 235. doi:10.1007/978-3-319-28344-9.
5. Hale, L. M.; Trautt, Z. T.; Becker, C. A. *Modelling and Simulation in Materials Science and Engineering* **2018**, *26* (5), 055003. doi:10.1088/1361-651x/aabc05. <https://www.ctcms.nist.gov/potentials/system/Si/651x/aabc05>.
6. Cahangirov, S.; Topsakal, M.; Aktürk, E.; Şahin, H.; Ciraci, S. *Phys. Rev. Lett.* **2009**, *102*, 236804. doi:10.1103/PhysRevLett.102.236804.
7. Cahangirov, S.; Özçelik, V. O.; Xian, L.; Avila, J.; Cho, S.; Asensio, M. C.; Ciraci, S.; Ru-bio, A. *Phys. Rev. B* **2014**, *90*, 035448. doi:10.1103/PhysRevB.90.035448.
8. Lee, C.-C.; Fleurence, A.; Friedlein, R.; Yamada-Takamura, Y.; Ozaki, T. *Phys. Rev. B* **2013**, *88*, 165404. doi:10.1103/PhysRevB.88.165404.

9. Balamane, H.; Halicioglu, T.; Tiller, W. A. *Phys. Rev. B* **1992**, *46*, 2250–2279. doi:10.1103/PhysRevB.46.2250.
10. Lysogorskiy, Y.; Hammerschmidt, T.; Janssen, J.; Neugebauer, J.; Drautz, R. *Mod-elling and Simulation in Materials Science and Engineering* **2019**, *27* (2), 025007. doi:10.1088/1361-651x/aafd13.
11. Michelin, J. V.; Gonçalves, L. G.; Rino, J. P. *Journal of Molecular Liquids* **2019**, *285*, 488–499. doi:/10.1016/j.molliq.2019.04.076.
12. Cahangirov, S.; Sahin, H.; Le Lay, G.; Rubio, A. *Introduction to the Physics of Silicene and other 2D Materials*; Springer Cham, 2017; Vol. 930. doi:10.1007/978-3-319-46572-2.
13. Andrew, R. C.; Mapasha, R. E.; Ukpong, A. M.; Chetty, N. *Phys. Rev. B* **2012**, *85*, 125428. doi:10.1103/PhysRevB.85.125428.
14. Maździarz, M. *Materials* **2021**, *14* (3), . doi:10.3390/ma14030519.
15. Hohenberg, P.; Kohn, W. *Phys. Rev.* **1964**, *136*, B864–B871. doi:10.1103/PhysRev.136.B864.
16. Kohn, W.; Sham, L. J. *Phys. Rev.* **1965**, *140*, A1133–A1138. doi:10.1103/PhysRev.140.A1133.
17. Gonze, X.; Jollet, F.; Araujo, F. A.; Adams, D.; Amadon, B.; Applencourt, T.; Audouze, C.; Beuken, J.-M.; Bieder, J.; Bokhanchuk, A.; Bousquet, E.; Bruneval, F.; Caliste, D.; Côté, M.; Dahm, F.; Pieve, F. D.; Delaveau, M.; Gennaro, M. D.; Dorado, B.; Espejo, C.; Geneste, G.; Genovese, L.; Gerossier, A.; Giantomassi, M.; Gillet, Y.; Hamann, D.; He, L.; Jomard, G.; Janssen, J. L.; Roux, S. L.; Levitt, A.; Lherbier, A.; Liu, F.; Lukačević, I.; Martin, A.; Mar-tins, C.; Oliveira, M.; Poncé, S.; Pouillon, Y.; Rangel, T.; Rignanese, G.-M.; Romero, A.; Rousseau, B.; Rubel, O.; Shukri, A.; Stankovski, M.; Torrent, M.; Setten, M. V.; Troeye, B. V.; Verstraete, M.; Waroquiers, D.; Wiktor, J.; Xu, B.; Zhou, A.; Zwanziger, J. *Computer Physics Communications* **2016**, *205*, 106 –131. doi:10.1016/j.cpc.2016.04.003.

18. Gonze, X.; Amadon, B.; Antonius, G.; Arnardi, F.; Baguet, L.; Beuken, J.-M.; Bieder, J.; Bottin, F.; Bouchet, J.; Bousquet, E.; Brouwer, N.; Bruneval, F.; Brunin, G.; Cavignac, T.; Charraud, J.-B.; Chen, W.; Côté, M.; Cottenier, S.; Denier, J.; Geneste, G.; Ghosez, P.; Gi-antomassi, M.; Gillet, Y.; Gingras, O.; Hamann, D. R.; Hautier, G.; He, X.; Helbig, N.; Holzwarth, N.; Jia, Y.; Jollet, F.; Lafargue-Dit-Hauret, W.; Lejaeghere, K.; Marques, M. A.; Martin, A.; Martins, C.; Miranda, H. P.; Naccarato, F.; Persson, K.; Petretto, G.; Planes, V.; Pouillon, Y.; Prokhorenko, S.; Ricci, F.; Rignanese, G.-M.; Romero, A. H.; Schmitt, M. M.; Torrent, M.; van Setten, M. J.; Troeye, B. V.; Verstraete, M. J.; Zérah, G.; Zwanziger, J. W. *Computer Physics Communications* **2020**, *248*, 107042. doi:10.1016/j.cpc.2019.107042.
19. Bloch, F. *Zeitschrift für Physik* **1929**, *57*, 545–555. doi:10.1007/BF01340281.
20. Perdew, J. P.; Wang, Y. *Phys. Rev. B* **1992**, *45*, 13244–13249. doi:10.1103/PhysRevB.45.13244.
21. Hamann, D. R. *Phys. Rev. B* **2013**, *88*, 085117. doi:10.1103/PhysRevB.88.085117.
22. Hamann, D. R.; Wu, X.; Rabe, K. M.; Vanderbilt, D. *Phys. Rev. B* **2005**, *71*, 035117. doi:10.1103/PhysRevB.71.035117.
23. Maździarz, M.; Mościcki, T. *Materials* **2020**, *13* (13), 3022. doi:10.3390/ma13133022.
24. Maździarz, M. *2D Materials* **2019**, *6* (4), 048001. doi:10.1088/2053-1583/ab2ef3.
25. Maździarz, M.; Psiuk, R.; Krawczyńska, A.; Lewandowska, M.; Mościcki, T. *Archives of Civil and Mechanical Engineering* **2022**, *22* (4), 193. doi:10.1007/s43452-022-00513-6.
26. Hinuma, Y.; Pizzi, G.; Kumagai, Y.; Oba, F.; Tanaka, I. *Computational Materials Science* **2017**, *128*, 140–184. doi:10.1016/j.commatsci.2016.10.015.
27. Grimvall, G.; Magyari-Köpe, B.; Ozolinš, V.; Persson, K. A. *Rev. Mod. Phys.* **2012**, *84*, 945–986. doi:10.1103/RevModPhys.84.945.

28. Tadmor, E. B.; Miller, R. E. *Modeling Materials: Continuum, Atomistic and Multiscale Tech-niques*; Cambridge University Press, 2011; doi:10.1017/CBO9781139003582.
29. Maździarz, M.; Young, T. D.; Jurczak, G. *Archives of Mechanics* **2011**, 63 (5-6), 533. <http://am.ippt.pan.pl/am/article/view/v63p533>
30. Maździarz, M.; Gajewski, M. *Computer Modeling in Engineering & Sciences* **2015**, 105 (2), 123–150. doi:10.3970/cmesc.2015.105.123.
31. Plimpton, S. *Journal of Computational Physics* **1995**, 117 (1), 1 –19. doi:10.1006/jcph.1995.1039.
32. Stukowski, A. *Modelling Simul. Mater. Sci. Eng.* **2010**, 18, 015012. doi:10.1088/0965-0393/18/1/015012.
33. Tersoff, J. *Phys. Rev. B* **1988**, 37, 6991–7000. doi:10.1103/PhysRevB.37.6991.
34. Kumagai, T.; Izumi, S.; Hara, S.; Sakai, S. *Computational Materials Science* **2007**, 39 (2), 457–464. doi:10.1016/j.commatsci.2006.07.013.
35. Pun, G. P. P.; Mishin, Y. *Phys. Rev. B* **2017**, 95, 224103. doi:10.1103/PhysRevB.95.224103.
36. Lee, B.-J. *Calphad* **2007**, 31 (1), 95–104. doi:10.1016/j.calphad.2006.10.002.
37. Du, Y. A.; Lenosky, T. J.; Hennig, R. G.; Goedecker, S.; Wilkins, J. W. *physica status solidi (b)* **2011**, 248 (9), 2050–2055. doi:10.1002/pssb.201147137.
38. Stillinger, F. H.; Weber, T. A. *Phys. Rev. B* **1985**, 31, 5262–5271. doi:10.1103/PhysRevB.31.5262.
39. Zhang, X.; Xie, H.; Hu, M.; Bao, H.; Yue, S.; Qin, G.; Su, G. *Phys. Rev. B* **2014**, 89, 054310. doi:10.1103/PhysRevB.89.054310.
40. Justo, J. a. F.; Bazant, M. Z.; Kaxiras, E.; Bulatov, V. V.; Yip, S. *Phys. Rev. B* **1998**, 58, 2539–2550. doi:10.1103/PhysRevB.58.2539.

41. Psfogiannakis, G.; van Duin, A. C. *Surface Science* **2016**, *646*, 253–260. doi:10.1016/j.susc.2015.08.019. Surface science for heterogeneous catalysis, a special issue in Honour of Richard Lambert
42. Yu, J.; Sinnott, S. B.; Phillpot, S. R. *Phys. Rev. B* **2007**, *75*, 085311. doi:10.1103/PhysRevB.75.085311.
43. Zuo, Y.; Chen, C.; Li, X.; Deng, Z.; Chen, Y.; Behler, J.; Csányi, G.; Shapeev, A. V.; Thompson, A. P.; Wood, M. A.; Ong, S. P. *The Journal of Physical Chemistry A* **2020**, *124* (4), 731–745. doi:10.1021/acs.jpca.9b08723.
44. Yanxon, H.; Zagaceta, D.; Wood, B. C.; Zhu, Q. *The Journal of Chemical Physics* **2020**, *153* (5), 054118. doi:10.1063/5.0014677.
45. Lysogorskiy, Y.; Oord, C. v. d.; Bochkarev, A.; Menon, S.; Rinaldi, M.; Hammerschmidt, T.; Mrovec, M.; Thompson, A.; Csányi, G.; Ortner, C.; Drautz, R. *npj Computational Materials* **2021**, *7* (1), 97. doi:10.1038/s41524-021-00559-9.
46. Nye, J.; Nye, P. *Physical Properties of Crystals: Their Representation by Tensors and Matrices*; Oxford science publications; Clarendon Press, 1985.
47. Maździarz, M.; Gajewski, M. *Computer Modeling in Engineering & Sciences* **2015**, *105* (2), 123–150. doi:10.3970/cmcs.2015.105.123.
48. Yoo, S.; Lee, B.; Kang, K. *Nanotechnology* **2021**, *32* (29), 295702. doi:10.1088/1361-6528/abf26d.